High-Accuracy Calibration of a Visual Motion Measurement System for Planar 3-DOF Robots Using Gaussian Process

Sheng Yao, Hai Li, Kai Wang, and Xianmin Zhang

***Abstract*— Visual motion measurement systems (VMMSs) are widely used in robotics for pose estimation. A common characteristic of VMMSs is that the measurement repeatability is high, but the absolute measurement accuracy is relatively low, once a commercial lens with a large field of view is used. To improve the measurement accuracy of the VMMS for pose tracking of planar 3-degree-of-freedom (3-DOF) robots, a coarse-to-fine calibration method is presented in this paper. In this paper, after the VMMS is constructed, a degenerated perspective-n-point (DPnP) algorithm for pose estimation of 3-DOF robots is introduced. Then, an analytical calibration technique is implemented to obtain the camera intrinsic parameters required by the DPnP algorithm. Subsequently, a fine calibration step based on Gaussian process is developed to compensate the estimated pose of the DPnP algorithm. To investigate the effectiveness and performance of the proposed method, a series of the simulations and experiments are carried out on a planar 3-DOF robot. The results demonstrate that the proposed calibration method is quite robust and can improve the measurement accuracy up to 90.47%. Specifically, in a measurement field of view of 200 mm × 200 mm, the absolute errors of the 3-DOF pose obtained from the VMMS are reduced to below 0.03 mm and 0.016°.**

***Index Terms*— Visual motion measurement system, coarse-to-fine calibration, Gaussian process, planar 3-DOF robot, high-accuracy calibration.**

I. Introduction

OWING to the advantages of a large travel range and high positioning accuracy, three degree-of-freedom (3-DOF) macro-micro manipulator systems play a significant role in the field of precision engineering for micromanipulation [1], [2]. Concretely, the macro part of these systems normally aims to provide a decimeter-scale workspace, while the micro part achieves fine positioning with an accuracy down to the nanoscale [3]. The key to combining these elements in macro-micro manipulators is maintaining the positioning error of the macro part at a level that is smaller than the workspace of the micro part. In order to improve the positioning accuracy of the macro part within its full working range and achieve a good combination, a proper method to ensure large-range and high-precision measurements is required.

With the desirable properties of noncontact measurement capability, high resolution and strong expansibility, visual motion measurement systems (VMMSs) are a top candidate for multi-DOF pose measurements [4], [5]. In order to measure pose with high absolute accuracy, calibration procedures are indispensable. Generally, calibration in metrology is the process of adjusting the output of a measurement device to match a specified standard and perform properly. For VMMSs combine with single camera, pose estimation normally involves a rigid transformation relating the camera coordinates to coordinates of known geometric features, which is also known as the perspective-n-point (PnP) problem [6]. To solve the PnP problem, achieving accurate camera intrinsic parameters is essential. To date, many methods for calibrating camera models and acquiring the intrinsic parameters have been presented in the field of computer vision [7], [8]. However, when these intrinsic parameters are directly used to solve the PnP problem, the obtained absolute accuracy of the pose is normally much lower than the repeatability accuracy [9]. The possible reasons for this phenomenon are as follows: (1) the accuracy of the known geometric features used in the camera calibration is limited (i.e., the accuracy of the intrinsic parameters is limited); and (2) the feature extraction algorithm used in the PnP solution may generate randomness (e.g., environmental vibration and randomized manufacturing errors). In general, these kinds of errors are difficult to model or compensate with conventional techniques.

To reduce these kinds of measurement errors, a promising solution is to use a learning-based approach for the fine calibration of VMMSs. By learning a system model from experiential data directly, learning-based approaches can adapt to complex system behaviors that are difficult to represent with idealized analytical models or to be modeled in advance. Of the well-known machine learning approaches, the Ridge [10] and Lasso [11] methods are considered as typical regression analysis methods for modeling multi-feature problems. Although they are fast and straightforward with a good generalization capability, these models may exhibit underfitting that cannot effectively reduce measurement errors for VMMSs. Many researchers have also investigated image

Manuscript received January 2, 2019; revised February 8, 2019; accepted February 10, 2019. Date of publication February 26, 2019; date of current version August 6, 2019. This work was supported in part by the National Natural Science Foundation of China (NSFC) under Grant 51820105007, Grant U1501247, and Grant 51605166 and in part by the China Postdoctoral Science Foundation under Grant 2018M643072. The associate editor coordinating the review of this paper and approving it for publication was Dr. Rosario Morello. *(Corresponding author: Xianmin Zhang.)*

The authors are with the Guangdong Key Laboratory of Precision Equipment and Manufacturing Technology, South China University of Technology, Guangzhou 510640, China (e-mail: me syao@mail.scut.edu.cn; lihai68156560@163.com; wangkailuixi@163.com; zhangxm@scut.edu.cn).

Digital Object Identifier 10.1109/JSEN.2019.2901816

1558-1748 © 2019 IEEE. Personal use is permitted, but republication/redistribution requires IEEE permission.
See http://www.ieee.org/publications_standards/publications/rights/index.html for more information.

Authorized licensed use limited to: SOUTH CHINA UNIVERSITY OF TECHNOLOGY. Downloaded on February 16,2020 at 15:34:23 UTC from IEEE Xplore. Restrictions apply.

correction using neural network methods and showed a reduction in measurement error [12], [13]. However, neural network methods still suffer from a high computational cost and can exhibit accuracy issues when the population of training dataset is small [14]. Based on Bayesian inference, Gaussian Process (GP) uses lazy learning to predict a value for an unmeasured point, and the GP model does not require a large amount of training data because of its robustness and smoothness, which is thus efficient and suitable for regression problems with a small number of feature sizes and a small amount of training data. GP also has many useful properties such as a closed-form predictive distribution and wide expressivity that it can handle both linear and non-linear data [15]. In practice, as a result of their desirable performance, GP models have been employed in many research areas such as robot control [16], spectrometer calibration [17] and robot calibration [18]. Moreover, GP models are non-parametric models, which should perform properly in many situations with little effort dedicated to tune the GP model parameters. For VMMSs in macro-micro manipulator systems, only a few hundred data of residual measurement errors at positioning points will be collected as training data. Hence, the GP method is expected to work well for this application with a relatively small amount of training data.

In this study, a high-accuracy calibration method that can apparently improve the measurement accuracy of a VMMS for planar 3-DOF robots is developed. To realize a pose measurement of the 3-DOF robot, a monocular vision system is established and a degenerated PnP (DPnP) algorithm for planar 3-DOF pose estimation is introduced. Afterwards, a scheme for obtaining the intrinsic parameters of the camera is briefly described, and a method for compensating residual error using GP is given in detail. Finally, simulations and experiments are performed to demonstrate the feasibility and effectiveness of the proposed method.

The remainder of the paper is organized as follows. In Section II, the configuration of the VMMS and the DPnP algorithm are introduced. A process for high-accuracy coarse-to-fine calibration is presented in Section III. The validity of the proposed method is verified by simulations and experiments, as described in Section IV and Section V, respectively. Conclusions and discussions on future works are given in Section VI.

II. VMMS for Planar 3-DOF Robots

A. System Description

Planar parallel mechanisms enjoy the advantages of fast speed, strong load capability, and high positioning accuracy due to small accumulative errors through kinematic chains [19]. Therefore, planar robots with translational and orientational DOFs are increasingly being used in industry and have become ideal for micropositioning and alignment [20], [21].

As sketched in Fig. 1, the manipulator system consists of three main parts: a manipulator, motion control unit, and VMMS. A planar 3-DOF parallel robot acts as the prototype of macromanipulator, which is expected to load the micro part

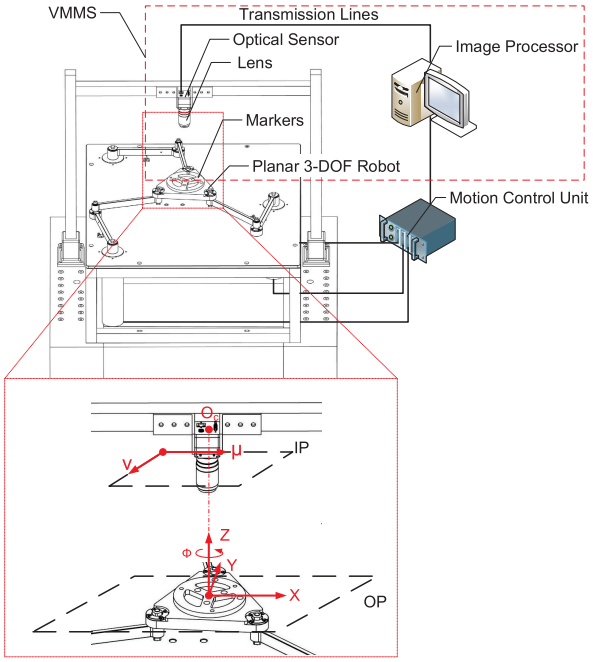

Fig. 1. Setup of the manipulation platform.

and provide coarse positioning in macro-micro manipulation. The motion control unit is used for trajectory planning and movement control. The VMMS, which is circled by a red dash line in Fig. 1, includes an optical lens, an optical sensor, markers, and an image processor. Images are captured through the high-resolution sensor and then transmitted to the image processor, where they are further processed and provide visual feedback to the control unit.

B. Degenerated Perspective-n-Point (DPnP) Algorithm for Pose Estimation of the 3-DOF Robot

As shown in the subfigure of Fig. 1, IP is the image plane, OP is the object plane, and O_c is the optical center. According to the pinhole model [22], the relationship between 2D points and 3D points can be written as

$$s\begin{bmatrix}\mu_i\\ \nu_i\\ 1\end{bmatrix} = \boldsymbol{A}\left[\boldsymbol{R}, \boldsymbol{T}\right]\begin{bmatrix}X_i\\ Y_i\\ Z_i\\ 1\end{bmatrix} \tag{1}$$

where i is a label for the points, 2D points in the IP are denoted by $p_i = (\mu_i, \nu_i)$, 3D points in the OP are denoted by $P_i = (X_i, Y_i, Z_i)$, s is an arbitrary scale factor, $\boldsymbol{A}$ is the camera intrinsic matrix, and $[\boldsymbol{R}, \boldsymbol{T}]$ are called the extrinsic parameters, which consist of a rotation and a translation [23]. Since the IP and OP are parallel in our VMMS, the number of independent parameters in $\boldsymbol{R}$ is degenerated to one, which is the rotation angle ϕ between the IP and OP coordinates. In this situation, we name solving this problem as solving the degenerated perspective-n-points (DPnP) problem.

Authorized licensed use limited to: SOUTH CHINA UNIVERSITY OF TECHNOLOGY. Downloaded on February 16,2020 at 15:34:23 UTC from IEEE Xplore. Restrictions apply.

In terms of Fig. 1 and Eq. (1), the projective equation of DPnP can be expressed as

$$s\begin{bmatrix}\mu_i\\ \nu_i\\ 1\end{bmatrix}=\begin{bmatrix}\alpha & 0 & \mu_0\\ 0 & \beta & \nu_0\\ 0 & 0 & 1\end{bmatrix}\begin{bmatrix}\cos\phi & \sin(\phi+\pi) & 0 & t_x\\ -\sin\phi & \cos(\phi+\pi) & 0 & t_y\\ 0 & 0 & -1 & t_z\end{bmatrix}\begin{bmatrix}X_i\\ Y_i\\ Z_i\\ 1\end{bmatrix} \tag{2}$$

where α and β are the scale factors for the μ and ν axes on the IP, (μ_0, ν_0) are the coordinates of the principal point, and (t_x, t_y, t_z) is the translational vector. Equating the last row of Eq. (2), we obtain $s = t_z$, and Eq. (2) can also be written as

$$\begin{bmatrix}\mu_i-\mu_0\\ \nu_i-\nu_0\end{bmatrix}=\begin{bmatrix}\frac{\cos\phi}{t_z}\alpha X_i-\frac{\sin\phi}{t_z}\alpha Y_i+\frac{t_x}{t_z}\alpha\\ -\frac{\sin\phi}{t_z}\beta X_i-\frac{\cos\phi}{t_z}\beta Y_i+\frac{t_y}{t_z}\beta\end{bmatrix} \tag{3}$$

To simplify Eq. (3) and remove the nonlinearity, let $a_1 = \frac{t_x}{t_z}$, $a_2 = \frac{t_y}{t_z}$, $a_3 = \frac{\sin\phi}{t_z}$, $a_4 = \frac{\cos\phi}{t_z}$, and we obtain the following equations

$$\begin{bmatrix}\mu_i-\mu_0\\ \nu_i-\nu_0\end{bmatrix}=\begin{bmatrix}a_1\alpha-a_3\alpha Y_i+a_4\alpha X_i\\ -a_2\beta-a_3\beta X_i+a_4\beta Y_i\end{bmatrix} \tag{4}$$

From the equations above, it can be seen that each point pair $(p_i \mapsto P_i)$ involves two constraints. Therefore, at least two control points are needed to obtain the parameters (a_1, a_2, a_3, a_4). By concatenating Eq. (4) for all n control points, we generate a linear system of the form

$$\underbrace{\begin{bmatrix}\alpha & 0 & -\alpha Y_1 & \alpha X_1\\ 0 & \beta & -\beta X_1 & -\beta Y_1\\ \vdots & \vdots & \vdots & \vdots\\ \alpha & 0 & -\alpha Y_n & \alpha X_n\\ 0 & \beta & -\beta X_n & -\beta Y_n\end{bmatrix}}_{\boldsymbol{C}}\underbrace{\begin{bmatrix}a_1\\ a_2\\ a_3\\ a_4\end{bmatrix}}_{\boldsymbol{a}}=\underbrace{\begin{bmatrix}\mu_1-\mu_0\\ \nu_1-\nu_0\\ \vdots\\ \mu_n-\mu_0\\ \nu_n-\nu_0\end{bmatrix}}_{\boldsymbol{b}} \tag{5}$$

After the intrinsic parameters are obtained from the coarse calibration, $\boldsymbol{a}$ can be solved, and the input of the GP model $[X_{in}, Y_{in}, \phi_{in}]$ can be calculated as

$$\begin{cases}X_{in}=t_x-t_{x0}\\ Y_{in}=t_y-t_{y0}\\ \phi_{in}=\phi-\phi_0\end{cases} \tag{6}$$

where $[t_{x0}, t_{y0}, \phi_0]$ are the initial values related to the robot's origin. Then, the mapping relationship between the IP and OP can be obtained after the fine calibration with GP compensation.

III. High-Accuracy Calibration Using Gaussian Process

A. Coarse Calibration to Obtain the Camera Intrinsic Parameters

Calibration is vital for VMMSs that require high a measurement accuracy within a large field of view. The goal of a vision system calibration is to identify the vision system model that minimizes the difference between measured and actual values.

The calibration process of the proposed VMMS consists of two steps. A coarse calibration is implemented using a method proposed in the literature [7], which is one of the most efficient analytic methods. Corner detection is used to extract control points from planar pattern images, in order to acquire the camera intrinsic and extrinsic parameters as shown in Eqs. (1) and (2). Since radial components are the main factor of lens distortion [24], the first two terms of the radial distortion coefficients k_1 and k_2 are considered, which can be formulated as

$$\begin{cases}\mu_i^u=\mu_i^d+(\mu_i^d-\mu_0)(k_1r_d^2+k_2r_d^4)\\ \nu_i^u=\nu_i^d+(\nu_i^d-\nu_0)(k_1r_d^2+k_2r_d^4)\\ r_d^2=\dfrac{(\mu_i^d-\mu_0)^2}{H^2}+\dfrac{(\nu_i^d-\nu_0)^2}{W^2}\end{cases} \tag{7}$$

where H is the height of the image, W is the width of the image, and (μ_0, ν_0), (μ_i^u, ν_i^u) and (μ_i^d, ν_i^d) represent the principal point, undistorted and distorted pixel image coordinates, respectively. The initial estimates of the distortion coefficients k_1 and k_2 are set to zero. Together with the intrinsic and extrinsic parameters, k_1 and k_2 can be refined through maximum likelihood estimation, which can be expressed by minimizing the following equation

$$\sum_{i=1}^{n}\sum_{j=1}^{m}\|\boldsymbol{m}_{ij}-f(\boldsymbol{A}, k_1, k_2, \boldsymbol{R}_i, \boldsymbol{t}_i, M_j)\| \tag{8}$$

where n is the image number, m is the control point number on each image, $\boldsymbol{m}_{ij}$ is image coordinate of control point, and $f(\boldsymbol{A}, k_1, k_2, \boldsymbol{R}_i, \boldsymbol{t}_i, M_j)$ is the projection of the control point M_j in image i in terms of Eqs. (1) and (7). To minimize Eq. (8), the Levenberg-Marquardt optimization algorithm is employed, and all parameters can be obtained.

B. Fine Calibration With GP Compensation for the Measurement System

After the coarse calibration in the first step to identify the best set of camera intrinsic parameters, there are still residual errors from geometric and non-geometric error sources that cannot be fully compensated by only changing the physical model parameters. Thus, Gaussian Process is employed to further calibrate the VMMS. Based on the intrinsic parameters and DPnP algorithm, the remaining residual error $\boldsymbol{\epsilon}$ can be written as $\boldsymbol{\epsilon} = \|\boldsymbol{P}_a - \boldsymbol{P}_m\|$ with the measured value $\boldsymbol{P}_m$ from the coarse calibration and actual value $\boldsymbol{P}_a$. Then, in the second step of the system calibration, the minimization problem that aims to minimize the overall error with GP compensation is presented as follows

$$min\|\boldsymbol{P}_a-\boldsymbol{P}_m-y(\boldsymbol{x})\| \tag{9}$$

where $y(\boldsymbol{x})$ is denoted as the GP model, and $\boldsymbol{x}$ is the input vector. The minimization problem formulated in Eq. (9) is then solved by computing the GP model.

Given a set of measurement residual errors, which is also the training data, our goal of GP regression is to make predictions of compensation values for unmeasured points. Generally, GP is defined as a probability distribution over functions $y(\boldsymbol{x})$ such that the set of values of $y(\boldsymbol{x})$ evaluated at an arbitrary set of inputs $\boldsymbol{x}_1, \boldsymbol{x}_2, \ldots, \boldsymbol{x}_N$ jointly have a Gaussian distribution. Thus, GP models the observations as a multivariate Gaussian

Authorized licensed use limited to: SOUTH CHINA UNIVERSITY OF TECHNOLOGY. Downloaded on February 16,2020 at 15:34:23 UTC from IEEE Xplore. Restrictions apply.

distribution, and any output from a new input can be predicted through Bayesian inference.

Given $(\boldsymbol{x}_i, y_i)$ as an input and output pair, where $\boldsymbol{x}_i \in R^{N\times 1}$, $y_i \in R$, then the multivariate Gaussian distribution model can be given by

$$\boldsymbol{y} \sim \mathcal{N}(0, \boldsymbol{K}) \tag{10}$$

where $\boldsymbol{K}$ is the $Gram$ matrix with size $N \times N$, and its elements are $k_{ij} = \phi(\boldsymbol{x}_i)^T\phi(\boldsymbol{x}_j) = k(\boldsymbol{x}_i, \boldsymbol{x}_j)$. A measure of the similarity between points, which is known as the kernel function, is introduced that allows us to implicitly use high-dimensional feature spaces without costly computation. This is an advantage of GP that we could consider covariance functions that only can be expressed in terms of an infinite number of basis functions $\phi(\boldsymbol{x}_i)$. The kernels largely influence the generalization properties of a GP model. With many excellent properties such as being stationary and infinitely differentiable, the Gaussian kernel is selected for the GP model due to its smoothness. Meanwhile, the polynomial kernel is a non-stationary kernel that allows the model to account for feature interactions, which can work well with limited training data. Combining the two kernels can lead to benefits from the properties of both kernels. This means that the resulting kernel will have a high value if either of the two base kernels has a high value [25]. Therefore, a Gaussian kernel combined with a polynomial kernel is used to determine $\boldsymbol{K}$, which can be formulated as

$$k_{ij} = \theta_0 exp(-\frac{\theta_1(\boldsymbol{x}_i - \boldsymbol{x}_j)^2}{2}) + (\theta_2 + \theta_3\boldsymbol{x}_i^T\boldsymbol{x}_j)^3 \tag{11}$$

where θ_i are hyperparameters that govern many aspects of the GP model including the length scale of correlations. Based on the evaluation of the likelihood function $p(\boldsymbol{y}|\boldsymbol{\theta})$, these hyperparameters can be learned from the data. A solution to estimate $\boldsymbol{\theta}$ is to maximize the log-likelihood function, which can be achieved by the conjugate gradient method, an efficient gradient-based optimization algorithm [26].

Then, given the observations $(\boldsymbol{x}, \boldsymbol{y})$ and a new input $\boldsymbol{x}_{N+1}$, the joint distribution over $y_1, y_2, \ldots, y_{N+1}$ is written by

$$\begin{bmatrix} \boldsymbol{y} \\ y_{N+1} \end{bmatrix} \sim \mathcal{N}(0, \boldsymbol{K}_{N+1}) \tag{12}$$

$$\boldsymbol{K}_{N+1} = \begin{bmatrix} \boldsymbol{K} & \boldsymbol{k}' \\ \boldsymbol{k}'^T & k_{N+1,N+1} \end{bmatrix} \tag{13}$$

where $\boldsymbol{K}$ is the $N \times N$ covariance matrix given by Eq. (8), the vector $\boldsymbol{k}'$ has a size of $N \times 1$ with elements $k(\boldsymbol{x}_i, \boldsymbol{x}_{N+1})$ for $i = 1, \ldots, N$, and the scalar $k_{N+1,N+1} = k(\boldsymbol{x}_{N+1}, \boldsymbol{x}_{N+1})$.

According to the property of conditional Gaussian distributions [27], the conditional distribution of the new output $p(y_{N+1}|\boldsymbol{y})$ is a Gaussian distribution with mean $m(\boldsymbol{x}_N+1)$ and covariance $\sigma^2(\boldsymbol{x}_N+)$ given by

$$y'|\boldsymbol{y} \sim \mathcal{N}(m(\boldsymbol{x}_N + 1), \sigma^2(\boldsymbol{x}_N + 1)) \tag{14}$$

$$m(\boldsymbol{x}_N + 1) = \boldsymbol{k}'\boldsymbol{K}^{-1}\boldsymbol{y} \tag{15}$$

$$\sigma^2(\boldsymbol{x}_N + 1) = k_{N+1,N+1} - \boldsymbol{k}'\boldsymbol{K}^{-1}\boldsymbol{k}'^T \tag{16}$$

Using the mean as the prediction value $y' = m(\boldsymbol{x}_N + 1)$, the output of any new input can be predicted based on known observations.

Since the residual error is distributed in the field of vision of the VMMS, it can be formulated as a function of the measurements $\boldsymbol{x} = [X_{in}, Y_{in}, \phi_{in}]$, which is also the input of the GP regression. Thus, the residual error is modeled that given the error $\boldsymbol{\epsilon}$ and the inputs $\boldsymbol{x}$, if new inputs $\boldsymbol{x}'$ are presented, the error $\boldsymbol{\epsilon}_i'(i = 1, 2, 3)$ can be predicted by Eq. (14), which can be rewritten as

$$\boldsymbol{\epsilon}_i'|\boldsymbol{\epsilon} \sim \mathcal{N}(\boldsymbol{k}'\boldsymbol{K}^{-1}\boldsymbol{\epsilon}, k_{N+M,N+M} - \boldsymbol{k}'\boldsymbol{K}^{-1}\boldsymbol{k}'^T) \tag{17}$$

where N and M are the number of inputs in the training dataset and new inputs, respectively. Then, the minimization problem in Eq. (9) is solved by finding the GP model that maps from $\boldsymbol{x}$ to $\boldsymbol{\epsilon}$, and the compensation $y(\boldsymbol{x}')$ of the error in the entire field of view of the VMMS is obtained.

IV. Simulation and Results

The simulation focuses on testing the calibration performance when the acquired images are distorted and contaminated by non-geometric factors. The camera model with distortion and sensor noise and the manufacturing error of the calibration object are simulated using the package presented in [28]. After the coarse calibration, GP modeling and prediction are implemented based on the scikit-learn framework [29].

As comparisons with the proposed GP method, the inverse distance weighting (IDW) method [30], Ridge regression [10] and Lasso method [11] are employed in fine calibration. Concretely, IDW is applied for multivariate interpolation. With a weighted average of the residual error values available at measured points, the compensation of IDW at any target point can be calculated as

$$\begin{cases} \boldsymbol{\epsilon}_0 = \sum_{i=1}^{n} w_i\boldsymbol{\epsilon}_i \\ w_i = f(d_i)/\sum_{i=1}^{n} f(d_i) \\ f(d_j) = 1/d_i^2 \end{cases} \tag{18}$$

where w_i is the weight of the ith measured point, d_i is the distance between the target point (x_0, y_0) and the measured point (x_i, y_i), $\boldsymbol{\epsilon}_i$, and $\boldsymbol{\epsilon}_0$ represent the residual errors at measured points and target points, respectively. Moreover, to maximize the performance of Ridge regression and Lasso method, an exhaustive grid search [31] and LARS algorithm [32] are adopted, respectively, which are also state-of-the-art approaches for setting the best regularization parameters.

In the simulation, a total of 300 training data points are randomly generated, and a 10-fold cross-validation is first performed as shown in Fig. 2, which shows that the proposed GP method for fine calibration can significantly improve the measurement accuracy, surpassing the other methods. Instead of exhibiting an oscillation like the other approaches, the proposed method shows stronger robustness with different training data. Since the final measurement errors in the 10-fold cross-validation are the smallest and most stable, there is no sign of overfitting when using the GP method.

Authorized licensed use limited to: SOUTH CHINA UNIVERSITY OF TECHNOLOGY. Downloaded on February 16,2020 at 15:34:23 UTC from IEEE Xplore. Restrictions apply.

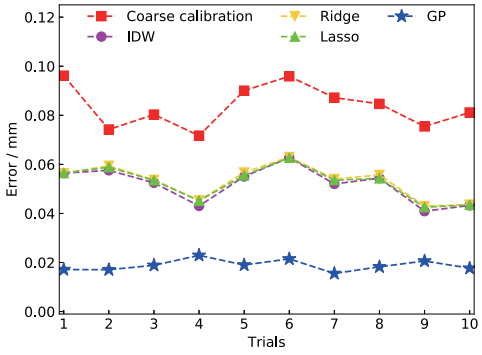

Fig. 2. 10-fold cross-validation of the training data, comparing other methods and GP using simulation data.

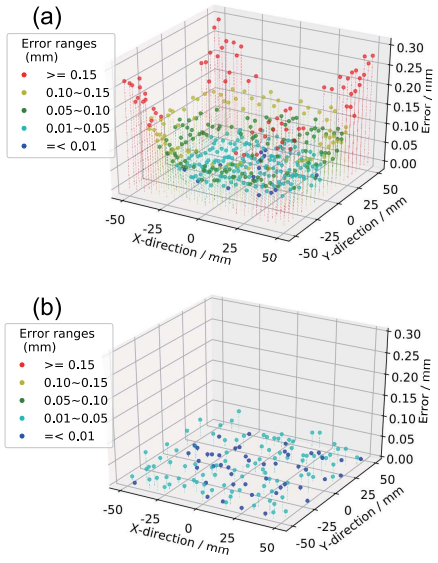

Fig. 3. Measurement errors in the position (a) after the coarse calibration and (b) after the fine calibration with the simulation data.

Subsequently, all 300 training data are used to obtain the fine calibrated model of the VMMS. Then, the updated model is tested with a testing data set containing 140 testing data. The results corresponding to coarse and fine calibrations are visualized in Figs. 3 and 4, and the data are categorized into different error ranges with different color markers. Generally, the further away from the optical axis of the VMMS, the larger the residual error after coarse calibration is. The measurement exhibits considerably large errors after the coarse calibration, which has a large number of errors exceeding 0.1 *mm* in position and 0.03° in orientation. Inaccurate modeling of the analytic calibration method contributes to the residual error. Using the proposed GP method in the fine calibration, the measurement error dramatically decreases. According to the test dataset, all the measurement errors are suppressed within the range of $0-0.05$ *mm* and $0-0.03°$, respectively. As listed in Table I, the mean measurement errors of the VMMS drop from 0.0835 *mm* and 0.0208° to 0.0162 *mm* and 0.0058°. In other words, the proposed method reduces the absolute errors by 80.50% and 71.85% in the position and orientation components, and it delivers the best performance

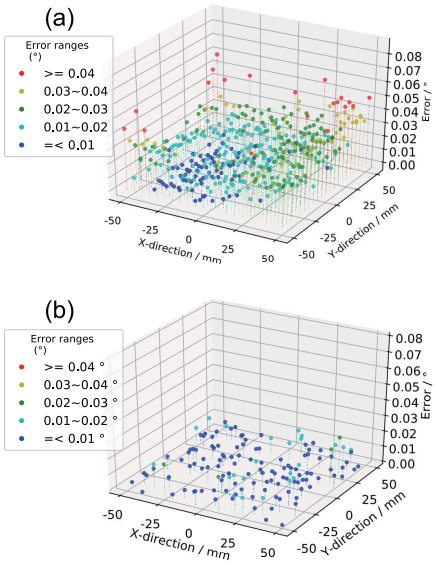

Fig. 4. Measurement errors in the orientation (a) after the coarse calibration and (b) after the fine calibration with the simulation data.

TABLE I
SIMULATION RESULTS FOR THE TEST DATASET

	Position		Orientation	
	Mean error	Improvement	Mean error	Improvement
Coarse	0.0835 *mm*	–	0.0208°	–
IDW	0.0487 *mm*	41.64%	0.0078°	62.15%
Ridge	0.0537 *mm*	35.68%	0.0075°	64.01%
Lasso	0.0534 *mm*	36.05%	0.0084°	59.72%
GP	0.0162 *mm*	80.50%	0.0058°	71.85%

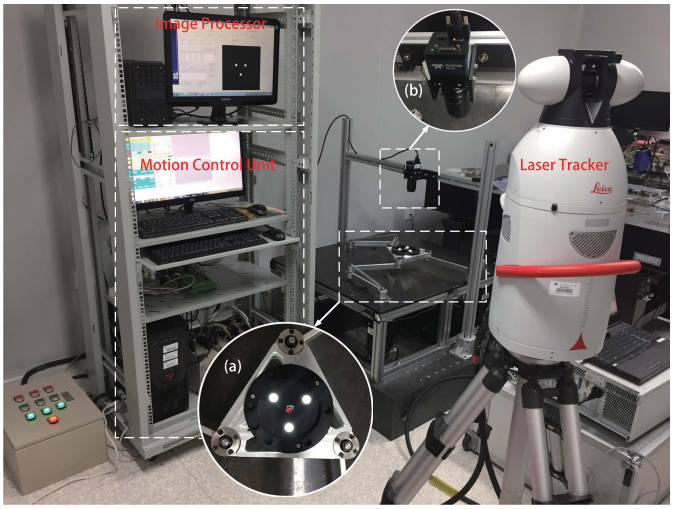

Fig. 5. The experiment setup. (a) A 3-RRR planar parallel manipulator, LED active markers, and a red-ring reflector for the laser tracker. (b) Lens and CMOS camera.

among all the considered two-step calibration methods based on the simulation data.

V. EXPERIMENT AND DISCUSSION

Experiments are carried out to demonstrate the practicability and reliability of the proposed method. As shown in Fig. 5, the experimental setup includes a planar 3-RRR

Authorized licensed use limited to: SOUTH CHINA UNIVERSITY OF TECHNOLOGY. Downloaded on February 16,2020 at 15:34:23 UTC from IEEE Xplore. Restrictions apply.

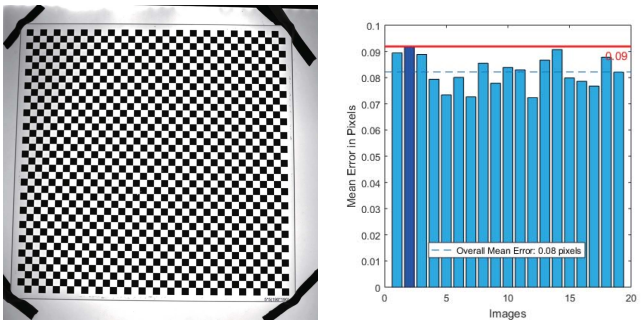

(a) (b)

Fig. 6. Coarse calibration of VMMS. (a) An image of the checkerboard. (b) The reprojection error. The red line represents the maximum reprojection error; the blue dashed line shows the average reprojection error.

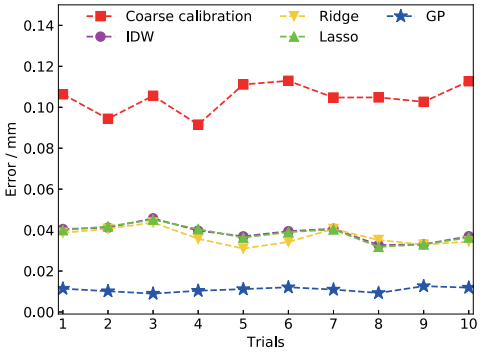

Fig. 7. 10-fold cross-validation of the training data, comparing the other methods and GP using the experimental data.

TABLE II
EXPERIMENT RESULTS FOR THE TEST DATASET

	Position		Orientation	
	Mean error	Improvement	Mean error	Improvement
Coarse	0.1079 mm	–	0.0208°	–
IDW	0.0370 mm	65.65%	0.0078°	62.15%
Ridge	0.0380 mm	64.75%	0.0075°	64.01%
Lasso	0.0402 mm	62.68%	0.0084°	59.72%
GP	0.0102 mm	90.47%	0.0056°	73.15%

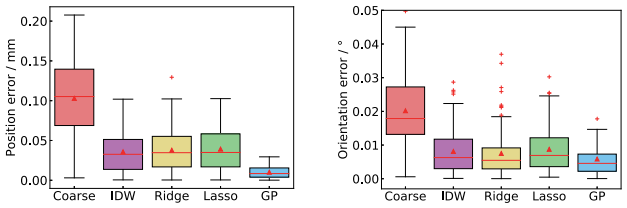

(a) (b)

Fig. 8. Comparison results of proposed method with other approaches using the boxplot representation. (a) The results on position. (b) The results on orientation.

(3-revolute-revolute-revolute) robot, a motion control unit, the VMMS, and a laser tracker (Leica Absolute Tracker AT901-B, measurement accuracy 5 μm, scanning angle 360°, scanning range $0 - 40$ m, scanning frequency 3000 Hz, angular resolution 0.14 $arcsecond$). Concretely, the motion control unit consists of a DMC-1886 motion control card, Yaskawa SGM7A-15AFA61 servo motors, the PICM-2900D interconnection module and an industrial personal computer. The VMMS has a $200mm \times 200mm$ field of view, and it consists of a Kowa LM16SC lens with the focal length of 16 mm, the Genie TS M2048 CMOS camera with a resolution of 2048×2048 mounted on a portal frame, an image processor (Intel(R) Core(TM) i7-4770M, CPU 2.40 GHz, RAM 4 GB), and three LED active markers. The nonparallelism of the IP and OP in the VMMS is analyzed in the previous work [33]. All experiments are conducted in an ISO Class 7 cleanroom to maintain a stable environment.

In the first step, the coarse calibration is conducted for the VMMS in Matlab. As shown in Fig. 6, the calibration object is a HongCheng HBM03-3020-5Q checkerboard with a 1 μm pattern accuracy. Fig. 6 also qualitatively illustrates the reprojection error after the coarse calibration. Each column presents the average reprojection error in each calibration image, while the dark blue column specifically shows the highest error among all reprojection errors. The red line and blue dashed line show the theoretical maximum and average reprojection errors after the coarse calibration, which are 0.09 pixels and 0.08 pixels, respectively.

In the second step, as shown in Fig. 5, a red-ring reflector of the laser tracker is mounted on the active marker, while the active marker is rigidly connected to the 3-RRR manipulator and their centroids coincide. The pose of the red-ring reflector will be tracked and recorded by the laser tracker system during the experiments. Then, keeping the 3-RRR robot at the original point, both the coordinates of the VMMS and the laser tracker system are initialized. The 3-RRR robot is controlled to move to each pose within the field of view, and the pose of the 3-RRR robot is measured by the VMMS and laser tracker system at the same time. Each pose is measured ten times by the VMMS to obtain an average value. Then, the deviations between the VMMS results and laser tracker results are acquired as residual errors. After collecting 300 measurement errors as training data, a 10-fold cross-validation is performed, and the calibrated VMMS models are obtained using the training data and four calibration methods.

The 10-fold cross-validation in Fig. 7 indicates that the proposed method possesses the strongest robustness and the smallest error among all the considered approaches. To validate the proposed method, all calibrated models are tested with a testing data set, which was not used to train the models, that consists of 140 new measurements. The results are shown in Table II and visualized in Fig. 8 using a boxplot representation.

As listed in Table II, the proposed method reduces the measurement errors by 90.47% and 73.15%, and the mean errors are reduced from 0.1079 mm and 0.0208° to 0.0102 mm and 0.0056°, respectively. As a reliable descriptive statistical method, the boxplot representation in Fig. 8 denotes the first (Q1) and third quartiles (Q3) of the error with boxes. While the vertical lines (whiskers) extending from the boxes represent the maximum and minimum, the horizontal red line is defined as the median of the data. In addition, the red triangle markers inside the boxes denote mean values, and

Authorized licensed use limited to: SOUTH CHINA UNIVERSITY OF TECHNOLOGY. Downloaded on February 16,2020 at 15:34:23 UTC from IEEE Xplore. Restrictions apply.

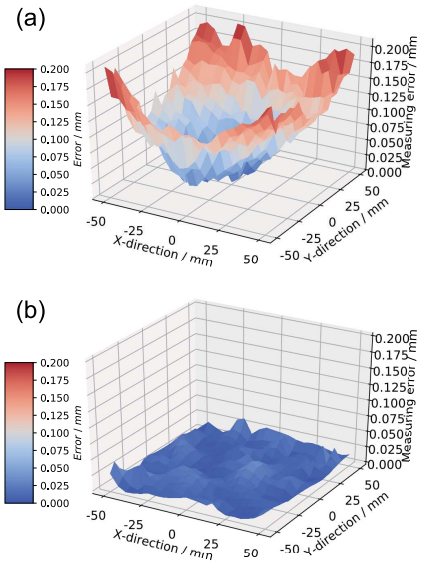

Fig. 9. Measurement errors in the position (a) after the coarse calibration and (b) after the fine calibration with the experimental data.

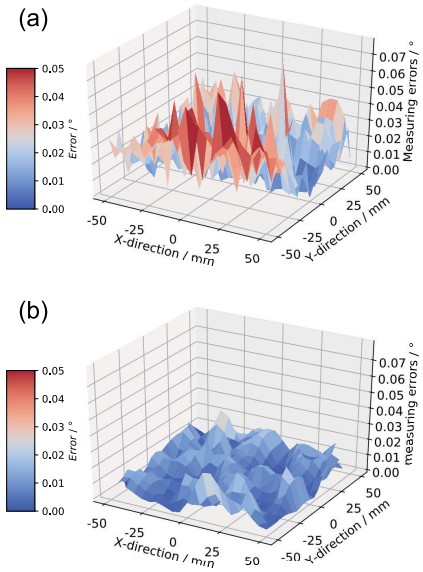

Fig. 10. Measurement errors in the orientation (a) after the coarse calibration and (b) after the fine calibration with the experimental data.

the red crosses outside boxes are extreme outliers. It can be seen that the proposed method possesses the smallest median and the shortest box height for both position and orientation, which indicates the lowest maximum error compared with the other four methods. For the position measurement, the proposed method dominate all indices in boxplot with a massive performance improvement, and even the peak value is almost smaller than the medians of the other methods. Since the DPnP algorithm already has a very high measurement accuracy for orientation, the improvement in the orientation is not as large as that for position after the calibration. Nevertheless, the proposed method still has the fewest extreme outliers, while other approaches have many outliers and suffer from reliability problems, indicating the high robustness of the proposed method in estimating robot pose.

Figs. 9 and 10 present the error distributions after coarse calibration and after fine calibration. As can be seen from Fig. 9, the residual error is still relatively large after the coarse calibration, which reveals the necessity of the fine calibration. Moreover, the absolute error of the position component is noticeably larger when the measuring pose is near the border of the field of view of the VMMS, which means that the position measurement suffers more geometric error after the coarse calibration. In addition, since the geometric error is favorably reduced after coarse calibration and the DPnP algorithm already has a high measurement accuracy in orientation, the absolute error of the orientation component in Fig. 10 presents more randomness rather than symmetry, which indicates it is mainly affected by non-geometric factors. After the fine calibration using the GP method, the measurement errors in both position and orientation dramatically decrease, and the distributions of the measurement errors become flat in shape. Meanwhile, the error distributions become more homogeneous, and the peak values of the both position and orientation components drop rapidly from approximately 0.2 *mm* and 0.06° to 0.03 *mm* and 0.016°.

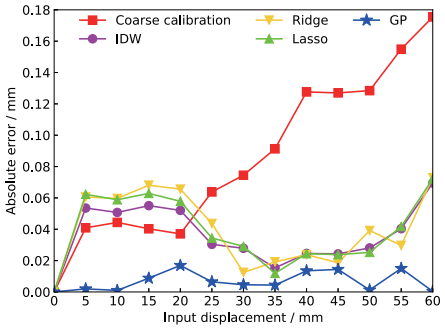

(a)

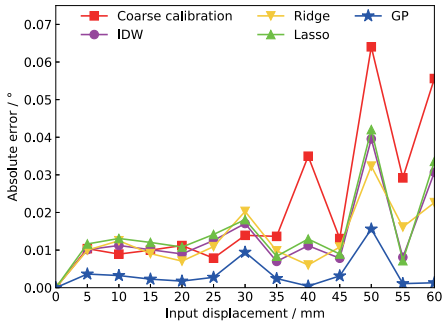

(b)

Fig. 11. Measurement accuracy of the calibrated system. (a) Absolute error of the position. (b) Absolute error of the orientation.

To further evaluate the improvement of the calibrated VMMS, the robot is controlled to input the displacements from the robot's origin within the range of $0-60\ mm$, and the measurement results are calculated based on different calibrated models. The data from the laser tracker system are also utilized as reference values to calculate the absolute error. Meanwhile, the standard deviation (SD) of ten measurement of each pose

Authorized licensed use limited to: SOUTH CHINA UNIVERSITY OF TECHNOLOGY. Downloaded on February 16,2020 at 15:34:23 UTC from IEEE Xplore. Restrictions apply.

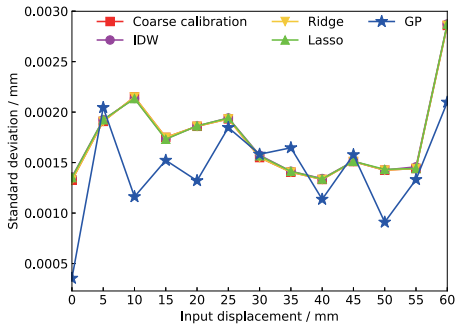

(a)

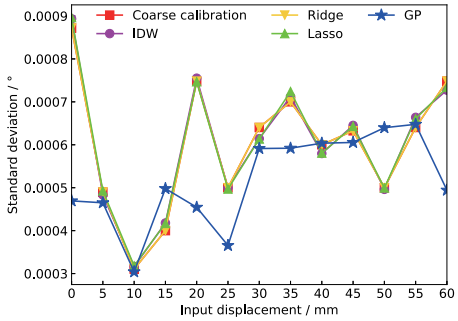

(b)

Fig. 12. Stability analysis of the calibrated system. (a) Standard deviation of the position. (b) Standard deviation of the orientation.

is calculated to analyze the stability of the VMMS. As shown in Fig. 11, using the proposed method, the absolute errors of both the position and orientation components decrease significantly. It also shows that the GP method always has the smallest measurement error compared to the other methods. Additionally, the IDW method, Ridge regression, and Lasso method overcompensate, even when their parameters are best tuned, while the GP method does not suffer from this issue. As displayed in Fig. 12, most SDs of the other methods are larger than that of the proposed method in both position and orientation, which verifies the high stability of the proposed method.

The results presented above show significant improvements for the calibrated VMMS using the proposed method, which yields the highest accuracy as well as more stable and reliable performance than other methods such as IDW, Ridge regression and Lasso. This demonstrates the adaptability, smoothness and robustness of the proposed method and that it has a strong capability to handle both geometric and non-geometric errors for VMMSs.

VI. Conclusion

This study presents a coarse-to-fine calibration method for high-precision measurements of the planar 3-DOF robot, which utilizes GP to minimize asymmetrical and nonlinear errors in VMMSs. The setup and measurement principle of the VMMS based on DPnP are introduced in detail, and a two-step calibration method is proposed for high-accuracy measurements in a large field of view. Furthermore, computational simulations and physical experiments are conducted to demonstrate the validity of the proposed method. The results show that the proposed method can effectively suppress measurement error and exhibit high stability. The results also indicate that the calibrated VMMS using the proposed method is capable of a successful combination of macro and micro manipulators during the macro-micro manipulation [3]. This study provides a competitive solution to the vision system calibration problem. We believe the proposed method will not only contribute to the development of macro-micro manipulator systems but will also enable more practical applications of GP in industry.

In future investigations, full-closed loop control of macro-micro manipulation based on the calibrated VMMS will be studied.

References

[1] M. Torralba, M. Valenzuela, J. A. Yagüe-Fabra, J. A. Albajez, and J. J. Aguilar, "Large range nanopositioning stage design: A three-layer and two-stage platform," *Measurement*, vol. 89, pp. 55–71, Jul. 2016.

[2] S. Fatikow, V. Eichhorn, F. Krohs, I. Mircea, C. Stolle, and S. Hagemann, "Development of automated microrobot-based nanohandling stations for nanocharacterization," *Microsyst. Technol.*, vol. 14, nos. 4–5, pp. 463–474, 2008.

[3] R. Wang and X. Zhang, "Parameters optimization and experiment of a planar parallel 3-DOF nanopositioning system," *IEEE Trans. Ind. Electron.*, vol. 65, no. 3, pp. 2388–2397, Mar. 2018.

[4] H. Li, X. Zhang, B. Zhu, and S. Fatikow, "Online precise motion measurement of 3-DOF nanopositioners based on image correlation," *IEEE Trans. Instrum. Meas.*, vol. 68, no. 3, pp. 782–790, Mar. 2019.

[5] G. Du and P. Zhang, "Online robot calibration based on vision measurement," *Robot. Comput.-Integr. Manuf.*, vol. 29, no. 6, pp. 484–492, 2013.

[6] J. A. Hesch and S. I. Roumeliotis, "A direct least-squares (DLS) method for PnP," in *Proc. Int. Conf. Comput. Vis.*, Nov. 2011, pp. 383–390.

[7] Z. Zhang, "A flexible new technique for camera calibration," *IEEE Trans. Pattern Anal. Mach. Intell.*, vol. 22, no. 11, pp. 1330–1334, Nov. 2000.

[8] C. Ricolfe-Viala, A.-J. Sanchez-Salmeron, and A. Valera, "Efficient lens distortion correction for decoupling in calibration of wide angle lens cameras," *IEEE Sensors J.*, vol. 13, no. 2, pp. 854–863, Feb. 2013.

[9] H. Li, X. Zhang, H. Wu, and J. Gan, "Line-based calibration of a micro-vision motion measurement system," *Opt. Lasers Eng.*, vol. 93, pp. 40–46, Jun. 2017.

[10] A. Gusnanto, Y. Pawitan, J. Huang, and B. Lane, "Variable selection in random calibration of near-infrared instruments: Ridge regression and partial least squares regression settings," *J. Chemometrics*, vol. 17, no. 3, pp. 174–185, 2003.

[11] R. Tibshirani, "Regression shrinkage and selection via the lasso: A retrospective," *J. Roy. Statist. Soc., Ser. B, Statist. Methodol.*, vol. 73, no. 3, pp. 273–282, 2011.

[12] L. N. Smith and M. L. Smith, "Automatic machine vision calibration using statistical and neural network methods," *Image Vis. Comput.*, vol. 23, no. 10, pp. 887–899, 2005.

[13] P. Cerveri, C. Forlani, N. A. Borghese, and G. Ferrigno, "Distortion correction for X-ray image intensifiers: Local unwarping polynomials and RBF neural networks," *Med. Phys.*, vol. 29, no. 8, pp. 1759–1771, 2002.

[14] M. R. G. Meireles, P. E. M. Almeida, and M. G. Simoes, "A comprehensive review for industrial applicability of artificial neural networks," *IEEE Trans. Ind. Electron.*, vol. 50, no. 3, pp. 585–601, Jun. 2003.

[15] C. E. Rasmussen and C. K. I. Williams, *Gaussian Processes for Machine Learning*. Cambridge, MA, USA: MIT Press, 2006.

[16] D. Nguyen-Tuong and J. Peters, "Local Gaussian process regression for real-time model-based robot control," in *Proc. IEEE/RSJ Int. Conf. Intell. Robot. Syst.*, Sep. 2008, pp. 380–385.

[17] T. Chen, J. Morris, and E. Martin, "Gaussian process regression for multivariate spectroscopic calibration," *Chemometrics Intell. Lab. Syst.*, vol. 87, no. 1, pp. 59–71, 2007.

Authorized licensed use limited to: SOUTH CHINA UNIVERSITY OF TECHNOLOGY. Downloaded on February 16,2020 at 15:34:23 UTC from IEEE Xplore. Restrictions apply.

[18] W. Jing, P. Y. Tao, G. Yang, and K. Shimada, "Calibration of industry robots with consideration of loading effects using product-of-exponential (POE) and Gaussian process (GP)," in *Proc. IEEE Int. Conf. Robot. Autom.*, May 2016, pp. 4380–4385.
[19] J.-P. Merlet, "Jacobian, manipulability, condition number and accuracy of parallel robots," *J. Mech. Des.*, vol. 128, no. 1, pp. 199–206, 2005.
[20] A. Yu, I. A. Bonev, and P. Zsombor-Murray, "Geometric approach to the accuracy analysis of a class of 3-DOF planar parallel robots," *Mech. Mach. Theory*, vol. 43, no. 3, pp. 364–375, 2008.
[21] L. Ren, J. K. Mills, and D. Sun, "Trajectory Tracking Control for a 3-DOF Planar Parallel Manipulator Using the Convex Synchronized Control Method," *IEEE Trans. Control Syst. Technol.*, vol. 16, no. 4, pp. 613–623, Jul. 2008.
[22] R. Hartley and A. Zisserman, *Multiple View Geometry in Computer Vision*. Cambridge, U.K.: Cambridge Univ. Press, 2003.
[23] Y. An, B. Li, H. Hu, and X. Zhou, "Building an omnidirectional 3D color laser ranging system through a novel calibration method," *IEEE Trans. Ind. Electron.*, to be published.
[24] J. Wang, F. Shi, J. Zhang, and Y. Liu, "A new calibration model of camera lens distortion," *Pattern Recognit.*, vol. 41, no. 2, pp. 607–615, 2008.
[25] D. Duvenaud, "Automatic model construction with Gaussian processes," Ph.D. dissertation, Comput. Biol. Learn. Lab., Univ. Cambridge, 2014.
[26] J. Nocedal and S. J. Wright, "Conjugate gradient methods," in *Numerical Optimization*. 2006, pp. 101–134.
[27] C. M. Bishop, *Pattern Recognition and Machine Learning (Information Science and Statistics)*. New York, NY, USA: Springer-Verlag, 2006.
[28] D. Samper, J. Santolaria, and J. J. Aguilar. "Metrovisionlab toolbox for camera calibration and simulation." [Online]. Available: http://metrovisionlab.unizar.es
[29] F. Pedregosa *et al.*, "Scikit-learn: Machine learning in python," *J. Mach. Learn. Res.*, vol. 12, pp. 2825–2830, Oct. 2011.
[30] S. Yao, X. Zhang, J. Yu, and B. Zhu, "Error modeling and calibration of a 4$\underline{\text{R}}$RRR redundant positioning system," *Aip Adv.*, vol. 7, no. 9, 2017, Art. no. 095009.
[31] S. An, W. Liu, and S. Venkatesh, "Fast cross-validation algorithms for least squares support vector machine and kernel ridge regression," *Pattern Recognit.*, vol. 40, no. 8, pp. 2154–2162, 2007.
[32] B. Efron, T. Hastie, I. Johnstone, and R. Tibshirani, "Least angle regression," *Ann. Statist.*, vol. 32, no. 2, pp. 407–499, 2004.
[33] H. Li, X.-M. Zhang, L. Zeng, and Y.-J. Huang, "A monocular vision system for online pose measurement of a $_3$RRR planar parallel manipulator," *J. Intell. Robot. Syst.*, vol. 92, no. 1, pp. 3–17, 2018.

Sheng Yao received the B.Eng. degree in mechatronic engineering from the South China University of Technology, Guangzhou, China, in 2016, where he is currently pursuing the Doctoral degree with the Guangdong Key Laboratory of Precision Equipment and Manufacturing Technology.

His research interests include high-precision vision systems for micromanipulation, vision-based control, and automation of robotic systems.

Hai Li received the Ph.D. degree from the South China University of Technology in 2018. He is currently a Post-Doctoral Researcher with the South China University of Technology. His research interests include vision-based precision measurements, visual servo control, and micro/nano manipulation.

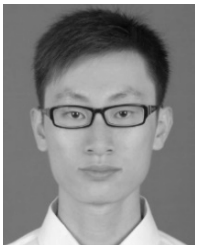

Kai Wang received the M.S. degree in software engineering from the South China University of Technology, in 2013, where he is currently pursuing the Ph.D. degree in mechanical manufacturing and automation. His research interests include robot kinematics, robot adaptation system, and human–robot cooperation and interaction.

Xianmin Zhang received the Ph.D. degree from the Beijing University of Aeronautics and Astronautics, Beijing, China, in 1993.

He has been the Director of the Guangdong Key Laboratory of Precision Equipment and Manufacturing Technology, since 2010, and he has been the Dean and the Chair Professor of the School of Mechanical and Automotive Engineering with the South China University of Technology, since 2013. He has finished over 50 projects and authored or co-authored over 300 technical papers and over 100 patents His research interests include robotics, precision instrument analysis and design, dynamics, and vibration control of mechanisms. He has been the Chair of the China Committee of IFToMM (International Federation for the Promotion of Mechanism and Machine Science) since 2016.

Authorized licensed use limited to: SOUTH CHINA UNIVERSITY OF TECHNOLOGY. Downloaded on February 16,2020 at 15:34:23 UTC from IEEE Xplore. Restrictions apply.